Hybrid QM/QM simulations of photochemical reactions in the molecular crystal N-salicylidene-2-chloroaniline

Post-print of a peer-reviewed article published by the Royal Society of Chemistry.
Published article available at: http://dx.doi.org/10.1039/C3CP51263K

Cite as:
Morrison, C., Kochman, M., & Bil, A. (2013). Hybrid QM/QM simulations of photochemical reactions in the molecular crystal N-salicylidene-2-chloroaniline. *Physical Chemistry Chemical Physics,* 15, 10803-10816.

Manuscript received: 25/03/2013; Accepted: 13/05/2013; Article published: 14/05/2013

Hybrid QM/QM simulations of photochemical reactions in the molecular crystal *N*-salicylidene-2-chloroaniline**†

Michał A. Kochman,[1] Andrzej Bil[2,3] and Carole A. Morrison[1,*]

[1]EaStCHEM, School of Chemistry, Joseph Black Building, University of Edinburgh, West Mains Road, Edinburgh, EH9 3JJ, UK.

[2]Institute of Physical Chemistry, University of Zürich, Winterthurerstrasse 190, CH-8057 Zürich, Switzerland.

[3]Faculty of Chemistry, University of Wrocław, F. Joliot-Curie 14, 50-383 Wrocław, Poland.

[*]Corresponding author; e-mail: C.Morrison@ed.ac.uk

[**]M. A. Kochman gratefully acknowledges the University of Edinburgh and the Centre for Numerical Algorithms and Intelligent Software (NAIS) for the award of a Principals Career Development Scholarship. Andrzej Bil would like to thank the Scientific Exchange Programme between the New Member States of the EU and Switzerland for financial support. We would like to thank Dr David Rogers from the Research Computing Facility at the University of Edinburgh School of Chemistry for his valuable advice. This work made use of the EaSTCHEM Research Computing Facility (http://www.eastchem.ac.uk/rcf) and the Edinburgh Compute and Data Facility (ECDF) (http://www.ecdf.ed.ac.uk/). The calculations with TURBOMOLE were performed at the Wrocław Network and Supercomputing Center. We also wish to acknowledge the use of the EPSRC funded Chemical Database Service at Daresbury.

[†]Celebrating 300 years of Chemistry at Edinburgh

Supporting information:
‡ Electronic supplementary information (ESI) available. See http://dx.doi.org/10.1039/C3CP51263K

Graphical abstract:

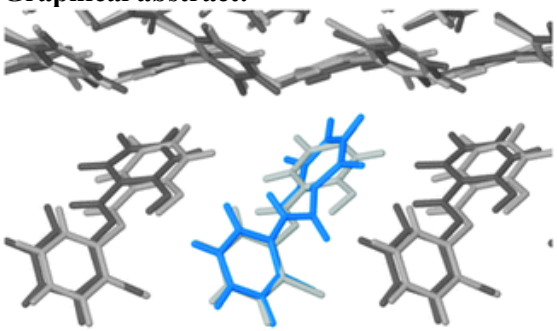

Abstract

In this paper, we report the application of the QM/QM hybrid simulation technique to the photoisomerisation reactions of anils (*i.e.*, Schiff bases of salicylaldehyde with aniline derivatives) in the solid state, on the example of the photochromic polymorph of*N*-salicylidene-2-chloroaniline. By propagating molecular dynamics on a potential energy surface constructed using a combination of time-dependent DFT and ground-state DFT calculations, two reaction pathways of the *cis*-enol isomer were observed, which occur with approximately equal probability. In the first pathway, the photoexcited molecule undergoes an intramolecular proton transfer reaction on average 25 fs after photoexcitation. It then persists in the *cis*-keto form for a few hundred femtoseconds before undergoing a pedal motion through which it reaches an S_1/S_0 conical intersection. This pathway, whose existence has previously been proposed in the literature to rationalize the feasibility of the photoisomerisation reaction in the confined environment of the crystal lattice, is predicted to lead to the formation of the *trans*-keto form. The second pathway is nonreactive and is analogous to a previously characterised radiationless de-excitation pathway of the isolated molecule. The *cis*-enol to *trans*-keto photoisomerisation is reversible. Following the photoexcitation of a *trans*-keto molecule, it persists in a largely unchanged geometry for a period of time ranging from a few hundred femtoseconds to over a picosecond, and subsequently undergoes a pedal motion in the same direction as the one involved in the *cis*-enol to *trans*-keto photoisomerisation, leading to the *cis*-keto isomer through another S_1/S_0 conical intersection.

1. Background

Since the discovery of the photochromic properties of some anil crystals, that is to say, a reversible change in colouration brought about by the absorption of electromagnetic radiation, by Senier *et al.*[1,2] over a century ago, the photochemical reactions of anils and related molecules have enjoyed extensive experimental[3–13] and theoretical[10,11,14–16] attention. Surprisingly, despite the longstanding debate over the mechanism and the structure of the product species of the photochromic process in anil crystals,[5,8] relatively little effort has been made towards understanding the solid-state reaction mechanism using the methods of theoretical chemistry. In particular, to the best of our knowledge, a dynamical simulation of this reaction mechanism in its entirety has not previously been reported. Therefore, in the present work we have undertaken to study this mechanism using a recently reported variant of the QM/QM hybrid method[17] for the modelling of photochemical reactions in molecular crystals in which reactive molecules are disordered throughout a lattice of non-reactive, ground-state molecules. The crux of this method is the description of a reactive molecule and surrounding nonreactive molecules (which represent the bulk lattice) at different levels of *ab initio* theory, which enables the simultaneous treatment of the electronic excitation localised on the reactive molecule and the interactions of that molecule with the surrounding molecules in a periodic boundary condition framework. In what follows, the present state of research on the anil photoisomerisation reaction is reviewed briefly so as to

provide context for our simulations of the photochemical reaction in the model anil *N*-salicylidene-2-chloroaniline (SCA).

The relevant reactions of anils are shown in Figure 1 on the example of the simplest anil, *N*-salicylideneaniline (SA). The lowest-energy form of SA is the colourless *cis*-enol form, which exists in thermal equilibrium with the yellow *cis*-keto form. With increasing temperature, the population of the *cis*-keto form increases, giving rise to a stronger yellow colouration. This sensitivity to temperature of the equilibrium between the *cis*-enol and *cis*-keto forms is partially responsible for the thermochromic properties of SA and other anils in the solid state. Additionally, for some anil crystals at low temperatures, thermochromism also originates from the temperature dependence of the fluorescence spectra.[18]

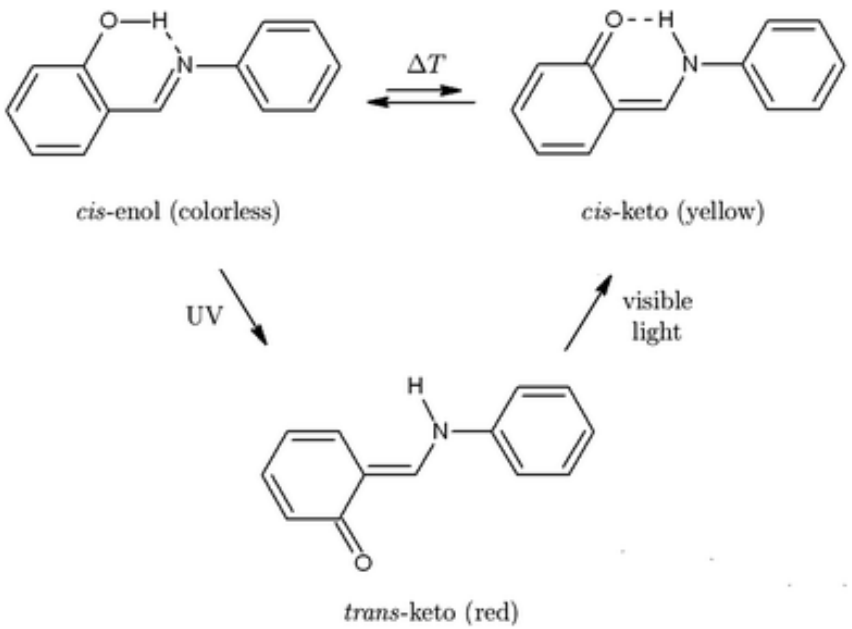

Figure 1. Thermo- and photochromic reactions of *N*-salicylideneaniline.

If the *cis*-enol form of SA is irradiated with UV light, a red *trans*-keto form is obtained. The reverse reaction is induced by visible light and leads to the *cis*-keto tautomer, which in turn is in thermal equilibrium with the *cis*-enol form. The mechanism of the *cis*-enol to *trans*-keto photoisomerisation in the isolated molecule of SA has been studied using DFT, time-dependent DFT (TD-DFT), CASPT2 and quantum dynamics simulations by Ortiz-Sánchez and coworkers.[16] The lowest singlet excited state (S_1) of the *cis*-enol form of SA was calculated to be a π, π^* state, in which the aniline group nitrogen is more basic relative to the salicylidene group oxygen. The S_1 surface of the *cis*-enol form was found to have two distinct reaction pathways, which are presented in Figure 2. Also, the S_1 and S_0 potential energy surfaces calculated by Ortiz-Sánchez *et al.* along both pathways are plotted schematically in Figure 3.

In the first pathway, the *cis*-enol molecule in the S_1 state undergoes rapid (with a decay time of 49.6 fs) excited-state intramolecular proton transfer (ESIPT) from the salicylidene group oxygen O1 to the aniline group nitrogen N1 which converts it into the *cis*-keto form. The molecule then undergoes a torsional motion of the salicylidene ring around the C3–C4 bond to reach a conical intersection (henceforth referred to as CI2) between S_0 and S_1. After passing through CI2, the molecule may be converted either to the *trans*-keto form or back to the *cis*-keto form; this internal conversion process was termed IC2 by Ortiz-Sánchez *et al*.

In the second pathway, through a torsional motion around the N1–C3 bond (see Figure 2 for atom numbering) the *cis*-enol molecule decays rapidly (with a decay time of 37.7 fs) through another S_0/S_1 conical intersection (which we label CI1), thus undergoing radiationless de-excitation to the ground state. Ortiz-Sánchez *et al.* termed this internal conversion process leading to recovery of the starting enol form in a somewhat deformed geometry as IC1.

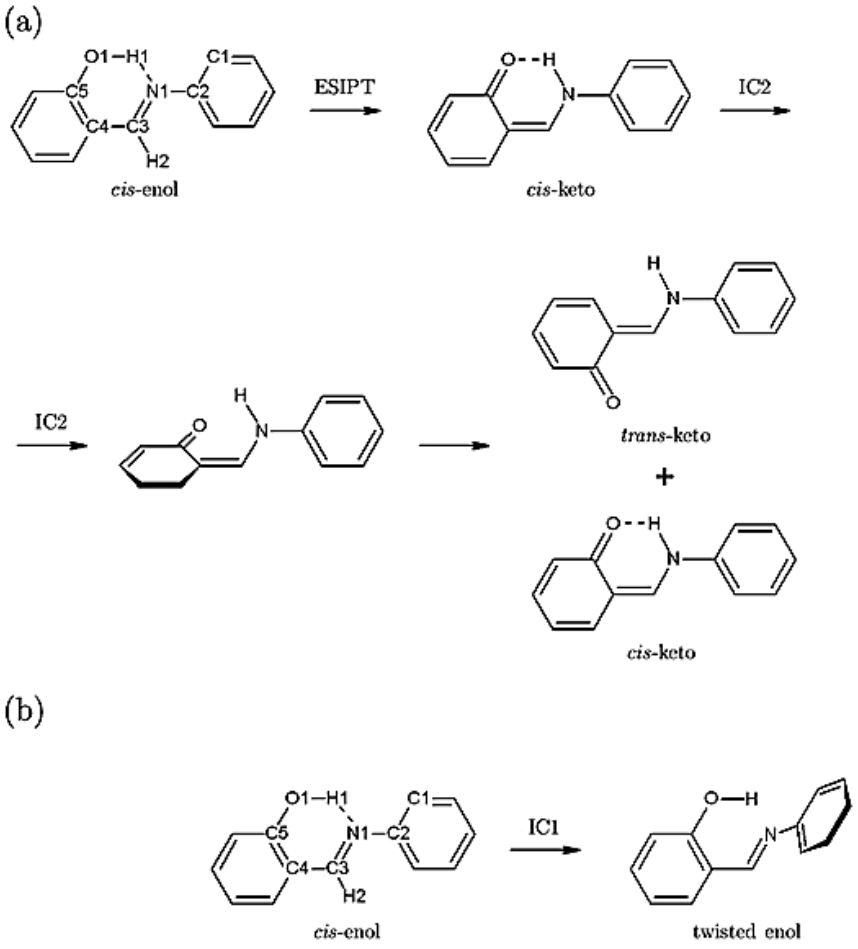

Figure 2.The two photoreaction pathways of the *cis*-enol form of the isolated *N*-salicylideneaniline molecule, based on calculations reported in Ref. 16. (a) ESIPT followed by IC2. (b) IC1.

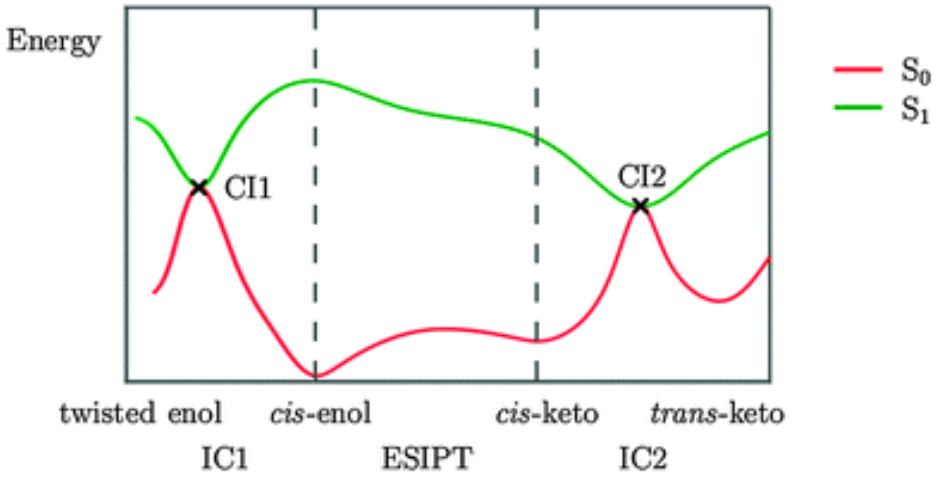

Figure 3. Schematic diagram of the S_0 and S_1 potential energy surfaces of the isolated *N*-salicylideneaniline molecule, based on calculations reported in Ref. 16. IC1, ESIPT and IC2 denote reaction coordinates representing the respective photochemical processes. The S_1/S_0 conical intersections involved in the radiationless deactivation processes IC1 and IC2 are labelled CI1 and CI2, respectively.

In the solid state, the ability of anils to undergo *cis*-enol to *trans*-keto photoisomerisation depends on the packing of the molecules within the crystal lattice. Extensive crystallographic studies[4,9,12] have shown that in order for an anil crystal to be photochromic, the lattice must be relatively uncrowded, while the constituent molecules must exist in a non-planar conformation and must not engage in intermolecular $\pi\cdots\pi$ interactions. Conversely, tightly-packed structures which exhibit π-stacking are not photochromic. In the case of some non-photochromic structures, the inability of molecules to undergo photoisomerisation can be ascribed to specific close contacts within the crystal lattice.[12]

The crystal structure of the *trans*-keto product of the anil photoisomerisation reaction was obtained for the first time by Harada *et al.*,[5] who also proposed a reaction mechanism (shown schematically in Figure 4 on the example of SCA) to explain the formation of the *trans*-keto isomer within the confined environment of the crystal lattice. According to this mechanism, following the initial photoexcitation and the subsequent ESIPT step, the *cis*-keto form is converted into the *trans*-keto form through a simultaneous torsion around the C2–N1 and C3–C4 bonds. This torsional motion is often called a "pedal" motion, due to its resemblance to the rotating pedals of a bicycle. The argument in favour of this mechanism is that the pedal motion requires less space within the crystal lattice than would be needed by a simple rotation of the salicylidene ring around the C3–C4 bond.

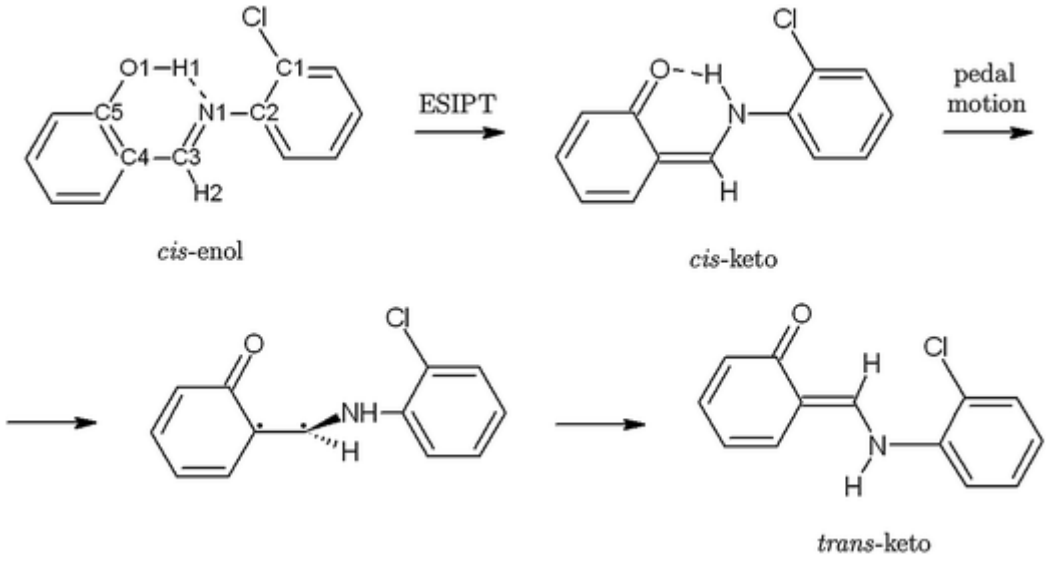

Figure 4. The solid-state *cis*-enol to *trans*-keto photoisomerisation mechanism of anils proposed by Harada *et al.*, shown on the example of SCA.

The difference in the mechanistic course of the anil photoisomerisation reaction in the isolated molecule and in the solid state provides an example of the directing influence of the bulk crystal structure on the reactivity of the individual component molecules, an effect that is also characteristic of many other photochemical reactions occurring in molecular crystals.[19–22] This, together with the potential technological applications of some anil crystals as optical materials,[23–25] makes this solid-state photoisomerisation reaction an interesting and important subject for theoretical study. In what follows, we describe the choice of the model compound under study in the present work and its crystal structure, before turning our attention to the QM/QM hybrid method that was employed to describe its dynamics.

2. Model system

We concerned ourselves with the photochromic polymorph of SCA whose crystal structure was reported by Bregman *et al.*,[26] and which has previously been presented as an example of a structure in which the photoisomerisation reaction is permitted by the packing of molecules.[8] Our choice was also motivated in part by the fact that it is one of the smallest anil molecules, with only a single substituent, which is an important consideration because of the steep scaling with system size of *ab initio* methods for the description of excited states.

The crystal structure of the photochromic polymorph of SCA is presented in Figure 5, where it can be seen that the crystal packing does not feature π-stacking interactions between molecules. In the individual

molecules, the chlorophenyl aromatic ring is twisted relative to the plane of the salicylidene ring. A least-squares mean plane was fitted to the carbon atoms comprising the chlorophenyl ring, and another to the carbon atoms comprising the salicylidene ring, within the computer program Mercury 3.0.[27] The two planes form a dihedral angle of 51.4°, which lies in the range of dihedral angle values from around 30° to around 50° that is typical of photochromic anils.[12] For a further discussion of the molecular packing in the photochromic polymorph of SCA, the Reader is referred to Section 1 of the ESI.‡ Here we state only the important conclusion that the crystal structure does not contain any voids near the aromatic rings of the SCA molecules, which suggests that a photoisomerisation mechanism involving a simple rotation around the C3–C4 bond would be likely to encounter significant steric obstruction, whereas the pedal-motion mechanism of Harada *et al.*, in which the two aromatic rings are less strongly displaced from their crystallographic positions, seems likely to be able to proceed with less steric hindrance.

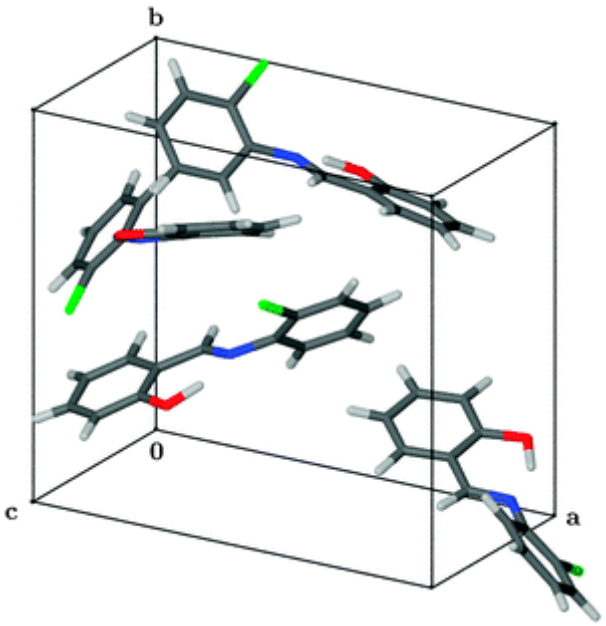

Figure 5. Crystal structure of SCA obtained at room temperature. The compound crystallizes in the orthorhombic space group $P2_12_12_1$ with one molecule in the asymmetric unit. a = 13.528 Å, b = 12.185 Å, c = 6.871 Å, Z = 4.

3 Computational methods

3.1 Outline of simulation scheme

In the present section we provide a synopsis of the computational scheme that was used to study the photochemical reactions in the SCA crystal.

1. Firstly, geometries of the *cis*-enol, *cis*-keto and *trans*-keto isomers of the isolated SCA molecule were optimised at the DFT level of theory, and $S_0 \rightarrow S_1$excitation energies were calculated using the TD-DFT method.

2. A 1 × 1 × 2 supercell of the photochromic SCA polymorph, representing the bulk lattice, was thoroughly equilibrated by means of molecular dynamics (MD) simulation in the canonical ensemble on the ground-state potential energy surface.

3. Following equilibration, phase space points (*i.e.*, sets of atomic coordinates and velocities) were sampled from the dynamics of the system at time intervals of 0.5 ps.

4. For each selected phase space point, photoexcitation to the S_1 state of a single molecule of SCA embedded within the crystal lattice was modeled by taking the system from the ground-state DFT potential energy surface to a hybrid QM/QM excited-state potential energy surface, in which the photoexcited molecule is treated using the TD-DFT method while the remaining molecules are described using ground-state DFT.

5. From each starting point generated in this manner, MD was propagated in the microcanonical ensemble on the hybrid QM/QM potential energy surface, thereby constituting a simulation of the photochemical reaction in the SCA crystal. The progress and outcome of the simulated trajectories was characterised by following several structural parameters, such as the proton transfer coordinate, the oxygen-nitrogen distance and the relevant torsion angles of the reactive molecule.

6. In order to test the correctness and accuracy of the TD-DFT method at predicting the S_1 potential energy surface of the SCA molecule, geometries of the photoexcited molecule were extracted from two representative system trajectories, and their energies were recalculated at the second-order approximate coupled cluster singles and doubles method (CC2) level of theory.

7. Having found that the simulated trajectories on the hybrid QM/QM potential energy surface show that the *cis*-enol to *trans*-keto isomerisation reaction in the SCA crystal proceeds through a mechanism involving the pedal motion, the same methodology was applied in order to model the reverse reaction. A 1 × 1 × 2 supercell of the photochromic polymorph was constructed with a single molecule in the *trans*-keto form and the remaining seven molecules in the *cis*-enol form, and the photochemical reaction of the *trans*-keto molecule was simulated by repeating steps 2 to 6 for that system.

The various components of the simulation are described in detail in the following subsections.

3.2 Construction of the simulated system

In the photoisomerisation reaction of anils in the solid state, the *trans*-keto isomer does not appear as a separate phase, but instead the *trans*-keto molecules are distributed in the lattice of unreacted *cis*-enol molecules in a disordered fashion.[5,8] As a result, in the case that only a small fraction of molecules undergo photoisomerisation, as is typical under experimental conditions, most reactive molecules are surrounded by nonreactive molecules. In order to reproduce these circumstances in the present theoretical study, simulations of the *cis*-enol to *trans*-keto photoisomerisation (which we will henceforth call the forward reaction) were carried out in the 1 × 1 × 2 supercell of the photochromic polymorph containing eight *cis*-enol molecules, of which only one was photoexcited. As the eight molecules contained in the supercell are related by symmetry, and therefore start off as equivalent, it does not matter which molecule we select as the photoexcited molecule. In Figure 6(a), we present the simulated system with the arbitrarily chosen photoexcited molecule drawn in blue. From now on, we will denote the entire simulated system, comprising the photoexcited molecule and the seven nonreactive molecules which represent the surrounding bulk lattice, as S while the photoexcited molecule alone will be referred to as C.

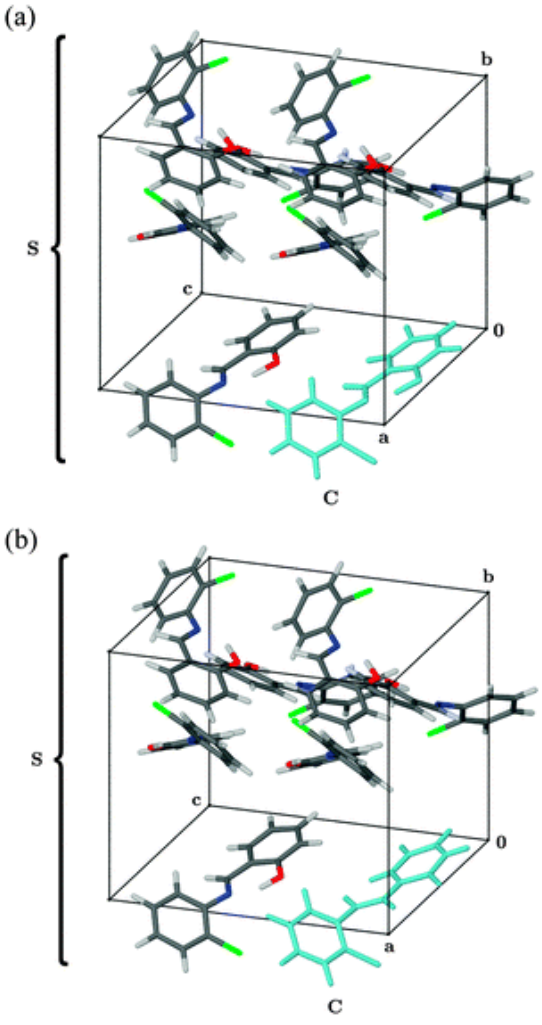

← ***Figure 6.*** Construction of the simulated system in the hybrid QM/QM simulations. S denotes the entire system while the photoexcited molecule, drawn in blue, is labelled C. (a) The 1 × 1 × 2 supercell of the photochromic polymorph of SCA used in the MD simulations of the forward reaction, shown at the geometry derived from experiment.[26] (b) The 1 × 1 × 2 supercell containing a single *trans*-keto molecule, used in the MD simulations of the reverse reaction, optimised at the DFT level of theory.

Likewise, simulations of the *trans*-keto to *cis*-enol photoisomerisation (the reverse reaction) were also carried out in a 1 × 1 × 2 supercell of the photochromic polymorph, but with one molecule converted into the *trans*-keto isomer. The procedure applied in order to "dock" the *trans*-keto molecule into the supercell is described in Section 2 of the ESI.‡ The resulting minimum-energy geometry of the 1 × 1 × 2 supercell containing one *trans*-keto molecule is illustrated in Figure 6(b).

Although this is not readily apparent in Figure 6, the photoexcited molecule within the 1 × 1 × 2 supercell of the photochromic polymorph of SCA is separated from periodic images of itself by nonreactive ground-state molecules. More formally, the shortest distance between the photoexcited molecule and its periodic images is fairly long, at 6.3 Å. We therefore believe that 1 × 1 × 2 supercell is a large enough system so as not to introduce periodic boundary conditions artefacts into the behaviour of the photoexcited molecule.

In the case of *N*-3,5-di-*tert*-butylsalicylidene-3-nitroaniline, the conversion of around 10% of the starting material into the *trans*-keto form resulted in only slight changes in the unit cell dimensions and very slight cell volume expansion (around 0.5%).[5] Therefore, as a simplifying approximation, the dimensions of the simulated 1 × 1 × 2 supercell were taken from the experimental structure[26] and were fixed throughout all MD simulations.

3.3 The QM/QM hybrid method

Because the simulated system contains a clearly defined reaction site (the reactive photoexcited molecule), while the surrounding molecules representing the bulk lattice do not directly participate in the reaction, it naturally lends itself to the application of a previously reported implementation of the subtractive QM/QM hybrid simulation method,[17] whereby the photoexcited molecule and the surrounding molecules are treated using time-dependent density functional theory (TD-DFT) and ground-state density functional theory (DFT), respectively. Here we briefly summarise the main features of this method, which we shall henceforth refer to as TD-DFT/DFT, and refer the reader to our previous work for a more detailed discussion.

The TD-DFT/DFT method is an adaptation of the subtractive QM/MM scheme[28] for the purpose of simulating photochemical reactions in molecular crystals at a model chemistry based exclusively on *ab initio* methods. Within the TD-DFT/DFT computation, the photoexcited molecule is treated using TD-DFT with a Gaussian-type orbital set, while the surrounding molecules are described using a periodic ground-state DFT calculation coupled with a plane-wave basis set, with the atomic cores replaced by pseudopotentials. The potential energy surface for the entire system is constructed using the following expression:

$$E_{\text{TD-DFT/DFT}}(\text{S}) = E^{\text{PW}}{}_{\text{DFT}}(\text{S}) + E^{\text{GTO}}{}_{\text{TD-DFT}}(\text{C}) - E^{\text{PW}}{}_{\text{DFT}}(\text{C}) \qquad (1)$$

Here, the subscripts TD-DFT and DFT refer to the electronic structure methods, while the superscripts PW (plane wave) and GTO (Gaussian-type orbital) refer to the basis sets used for the evaluation of the respective terms.

The term $E^{PW}_{DFT}(S)$ represents the potential energy of the entire system evaluated through a periodic ground-state DFT calculation. It includes all interactions between the photoexcited molecule and the surrounding bulk lattice, and as such the TD-DFT/DFT simulation treats these interactions as though the photoexcited molecule was in the electronic ground state, which is an approximation of the subtractive QM/QM scheme.

$E^{GTO}_{TD\text{-}DFT}(C)$ and $E^{PW}_{DFT}(C)$ are the potential energies of the reactive molecule alone, evaluated respectively at the TD-DFT and DFT levels. Both these terms are calculated in the absence of the surrounding bulk lattice. As a consequence, in the TD-DFT/DFT calculation the reactive molecule does not experience the polarizing influence of the surrounding bulk lattice. This omission of the polarisation of the photoexcited molecule is another approximation inherent in the subtractive QM/QM scheme.

The term $E^{PW}_{DFT}(C)$ is subtracted from the sum $E^{PW}_{DFT}(S) + E^{GTO}_{TD\text{-}DFT}(C)$ in order to correct for the double counting of the intramolecular energy of the reactive molecule. It is evaluated at the same level of theory as $E^{PW}_{DFT}(S)$, except that in the term $E^{PW}_{DFT}(C)$ the reactive molecule C is treated as an isolated system.

3.4 Simulation setup

3.4.1 Isolated-molecule calculations

Geometry optimisations of the *cis*-enol, *cis*-keto and *trans*-keto isomers of the isolated SCA molecule were carried out at the DFT level of theory using the PBE0[29] exchange-correlation functional coupled with the 6-31G(d,p) basis set as implemented in the computational chemistry software package Gaussian 09.[30] Vertical $S_0 \rightarrow S_1$ excitation energies were calculated at the optimised geometries using the TD-DFT method. The same level of theory was applied in the calculation of the term $E^{GTO}_{TD\text{-}DFT}(C)$ in the TD-DFT/DFT simulations.

Our choice of the TD-DFT method for the treatment of the S_1 state of the photoexcited SCA molecule was dictated by the fact that it has previously been demonstrated to predict the topology of the potential energy surface of that state in good agreement with the multiconfigurational CASPT2 method,[16] as well as its superior computational efficiency as compared with wavefunction-based excited-state methods. A more in-depth analysis of the applicability of the TD-DFT method to describe the S_1 state is given below in Section 3.4.3.

3.4.2 Solid-state calculations

In the equilibration of the SCA 1 × 1 × 2 supercell in the ground electronic state, the potential energy of the system was evaluated using the Perdew, Burke, Ernzerhof exchange-correlation DFT functional[31] as implemented in the software package CASTEP Academic Release version 5.501.[32] The plane-wave cutoff was set at 450 eV. The electronic Brillouin zone was sampled by using a Monkhorst–Pack *k*-point grid with a *k*-point spacing of at most 0.1 $Å^{-1}$, achieved using a single *k*-point at the Γ-point (0 0 0). The default ultrasoft pseudopotentials were used.[33] Energies and forces were corrected for dispersion interactions using the semiempirical scheme of Grimme.[34] The SCF convergence threshold was set to 1.0×10^{-7} eV per atom. The same level of theory was applied in the evaluation of the term $E^{PW}_{DFT}(S)$ in the TD-DFT/DFT simulations.

When calculating the term $E^{PW}_{DFT}(C)$ in the hybrid TD-DFT simulations, the reactive molecule was placed in a cubic cell of edge length 20 Å, which was found to be large enough that the total energy did not change significantly on increasing the cell size further. The electronic Brillouin zone was sampled at the Γ-point only. The remaining calculation parameters were identical as in the evaluation of the term $E^{PW}_{DFT}(S)$.

Lastly, the term $E^{PW}_{DFT}(S)$ was evaluated using the TD-DFT method implemented within Gaussian 09[30] at the PBE0/6-31G(d,p) level of theory, with the reactive molecule C in the S_1 electronic state.

The system was equilibrated by propagating Born–Oppenheimer molecular dynamics in the canonical (NVT) ensemble for 4 ps, following a production run was carried out, which lasted 7.5 ps and 3.5 ps for the supercells used in the simulations of the forward and reverse reactions, respectively. Throughout the equilibration and production periods, the temperature was maintained at 280 K using a chain of five Nosè–Hoover thermostats with a relaxation time of $\tau = 1$ ps. A time step of 0.5 fs was used throughout the equilibration and production periods. Phase space points were collected from the production run at intervals of 0.5 ps starting from$t = 4$ ps to serve as starting points for the hybrid QM/QM simulations of the photochemical reaction, for a total of sixteen and eight starting points for the simulations of the forward and reverse reactions, respectively.

From each of these starting points, Born–Oppenheimer molecular dynamics in the microcanonical (*NVE*) ensemble was propagated on the hybrid TD-DFT/DFT potential energy surface defined by eqn (1), with the photoexcited molecule in the S_1 electronic state. These simulations were handled using a "wrapper" bash script, which created the Gaussian 09 and CASTEP input files, executed these programs, calculated the potential energy and the atomic forces, and integrated Newton's equations of motion. The force vector on the *i*th atom in the system was calculated as minus the gradient of the potential energy given by eqn (1) with respect to the Cartesian coordinates of that atom, resulting in the following expression for the force:

$$\mathbf{F}_i = \begin{cases} -\nabla_i E_{\mathrm{DFT}}^{\mathrm{PW}}(\mathbf{S}) - \nabla_i E_{\text{TD-DFT}}^{\mathrm{GTO}}(\mathbf{C}) + \nabla_i E_{\mathrm{DFT}}^{\mathrm{PW}}(\mathbf{C}) \text{ if atom } i \\ \quad \text{belongs to the photoexcited molecule } \mathbf{C} \\ -\nabla_i E_{\mathrm{DFT}}^{\mathrm{PW}}(\mathbf{S}) \text{ otherwise} \end{cases}$$

Newton's equations of motion were integrated using the Velocity Verlet scheme with a time step of 0.5 fs. On the grounds that previous studies of the ESIPT reaction in the structurally related molecule 2-(2′-hydroxyphenyl)benzothiazole[35,36] have characterised the proton transfer as a ballistic motion of the wave packet, with no significant involvement of proton tunneling, we believe the treatment of the shuttling proton as a classical point particle does not introduce large errors into our simulations of the photochromic polymorph of SCA. The system dynamics was propagated until the photoexcited molecule reached a S_1/S_0 conical intersection, which occurred in every simulated trajectory.

3.4.3 Assessment of the accuracy of the TD-DFT method

Methods such as DFT and TD-DFT are incapable of providing a qualitatively correct description of a potential energy surface near a conical intersection, where the molecular wavefunction has an inherent multiconfigurational character. Their usage may therefore generate simulation artefacts when the photoexcited molecule approaches a conical intersection, as happens in the photochemical reaction of SCA. Moreover, by analogy with the photochemical reactions of the molecules 2-(2′-hydroxyphenyl)benzothiazole[37] and 7-(2′-pyridyl)indole,[38] in both of which the ESIPT reaction is followed by a mutual twist of two aromatic rings, we may expect that during the torsional motions through which the SCA molecule reaches an S_1/S_0 conical intersection, the molecule adopts a strong biradicaloid character. Methods such as DFT and TD-DFT may incorrectly predict the charge distribution of a biradicaloid state, which represents another potential source of error in the hybrid TD-DFT/DFT simulations. These factors necessitate a critical evaluation of the ability of the TD-DFT method to describe the photochemical reaction of SCA.

Fortunately, Ortiz–Sánchez and coworkers[16] have provided evidence that the TD-DFT method is able to describe the S_1 potential energy surface surface of the SA molecule. In the work just cited, the TD-DFT method was found to predict the existence of two S_1/S_0 conical intersections (CI1 and CI2; see Figure 3 for the location of these conical intersections on the potential energy surface) involved in the isolated-molecule reaction mechanism, in the sense that near the conical intersection geometries, the energy gap between the S_0 and S_1 states becomes very small. Both these conical intersections were subsequently confirmed to exist, at geometries similar to the TD-DFT-derived geometries, at the CASPT2 level of theory, which is capable of providing a correct description of conical intersections as well as biradicals. Therefore, insofar as the results obtained for SA can be extrapolated to its derivative SCA, we believe that the use of the TD-DFT method to

describe the S_1 state of the SCA molecule is unlikely to lead to simulation artefacts such as spurious conical intersections.

Nevertheless, despite the demonstrated ability of the TD-DFT method to predict the existence and rough location of the relevant conical intersections of the SA molecule, we took effort to further assess the ability of the TD-DFT to describe the S_1 state of SCA. In order to achieve this, geometries of the photoexcited molecule were extracted from two representative MD trajectories generated on the TD-DFT/DFT potential energy surface (see Sections 4.3.1 and 4.3.2 for a full discussion of the two selected trajectories). The energies of the ground and excited states of the photoexcited molecule were subsequently calculated at the second-order approximate coupled-cluster (CC2) level of theory and compared with those computed using the TD-DFT method, which constitutes a *post factum*assessment of the performance of the TD-DFT method employed in the TD-DFT/DFT simulations. While the CC2 method itself, being a single-configurational method, is not capable of providing a description of conical intersections, and may also incorrectly predict the charge distribution of a biradicaloid state, in studies of ESIPT systems where it was benchmarked against multiconfigurational methods the CC2 method was found to correctly locate the relevant conical intersections, in that the energy gaps between the S_0 and S_1 states became small in the conical intersection regions.[37,39] The CC2 method is therefore not to be treated as an exact benchmark for the TD-DFT method, but rather it is meant to help identify a possible failure of TD-DFT to correctly describe the S_1 state. We may expect that any strong discrepancy between energies of the S_1 state between the TD-DFT and CC2 methods would indicate that either or both of these methods is yielding inaccurate results.

We remark here that instead of the CC2 method, it clearly would have been more appropriate to use a dynamically correlated multiconfigurational method such as CASPT2 to serve as a benchmark for the TD-DFT calculations. However, it is likely that a very extensive active space (larger than ten electrons in ten orbitals) would be necessary to provide an accurate description of the entire potential energy surface of the SA molecule.[16] In the present work, the energy of the photoexcited molecule is calculated along TD-DFT/DFT trajectories in which the photoexcited molecule undergoes large structural changes, thus exploring a sizeable area of the potential energy surface, and therefore due to computational limitations, we did not attempt to apply a multiconfigurational method.

The energies of the S_0 and S_1 states of the reactive SCA molecule were calculated through single-point calculations at the CC2[40] level of theory as implemented in the computational chemistry software package TURBOMOLE version 6.4,[41] taking advantage of the parallel implementation of the ricc2 program.[42,43] The frozen core and the resolution-of-the-identity approximations were used in all calculations. The cc-pVDZ basis set[44,45] was used for hydrogen, carbon and chlorine atoms, whereas for nitrogen and oxygen atoms, additional diffuse functions were applied by employing the aug-cc-pVDZ basis set.[46] The auxiliary basis set was cc-pVDZ for hydrogen, carbon and chlorine and aug-cc-pVDZ for nitrogen and oxygen.[47] Such single-

point CC2 calculations were performed along two representative trajectories on the TD-DFT/DFT potential energy surface at intervals of 10 fs, except during the final 50 fs of each trajectory, when the single-point calculations were performed at intervals of 5 fs.

4. Results and discussion

4.1 Energy minima of the isolated molecule

Geometries of the *cis*-enol, *cis*-keto and *trans*-keto isomers of SCA optimised at the PBE0/6-31G(d,p) level of theory are shown in Figure 7(a)–(c), respectively. In order to be able to monitor the conformational changes of the reactive molecule during simulations on the TD-DFT/DFT potential energy surface, we followed the four torsion angles ϕ(N1–C3–C4–C5), ϕ(C2–N1–C3–C4), ϕ(H2–C3–C4–C5) and ϕ(C1–C2–N1–C3) (see Figure 7(a) for atom numbering). The ground-state potential energies, $S_0 \rightarrow S_1$ vertical excitation energies calculated using the TD-DFT method, and values of the four torsion angles which describe the molecular conformation of the isomers of SCA are given in Table 1.

	***cis*-enol**	***cis*-keto**	***trans*-keto**
$E(S_0)$,[a] eV	0	0.253	0.905
$E(S_1) - E(S_0)$, eV	3.70	3.12	2.96
ϕ(N1–C3–C4–C5), °	0.7	−0.2	−176.4
ϕ(C2–N1–C3–C4), °	177.0	177.2	179.7
ϕ(H2–C3–C4–C5), °	−178.3	−178.9	2.1
ϕ(C1–C2–N1–C3), °	144.6	157.5	48.4

a The ground-state potential energy values are given relative to the *cis*-enol isomer and include zero-point vibrational energy.

Table 1. Summary of geometry optimisations for isomers of the isolated SCA molecule. (See Figure 7(a) for atom numbering.)

As can be read from Table 1, the *cis*-enol isomer is the lowest in energy, followed by the *cis*-keto, while the *trans*-keto is much higher in energy. In all three isomers, the hydroxyphenyl moiety and the atoms C2, N1, C3 lie roughly on the same plane, whereas the chlorophenyl moiety is twisted relative to that plane.

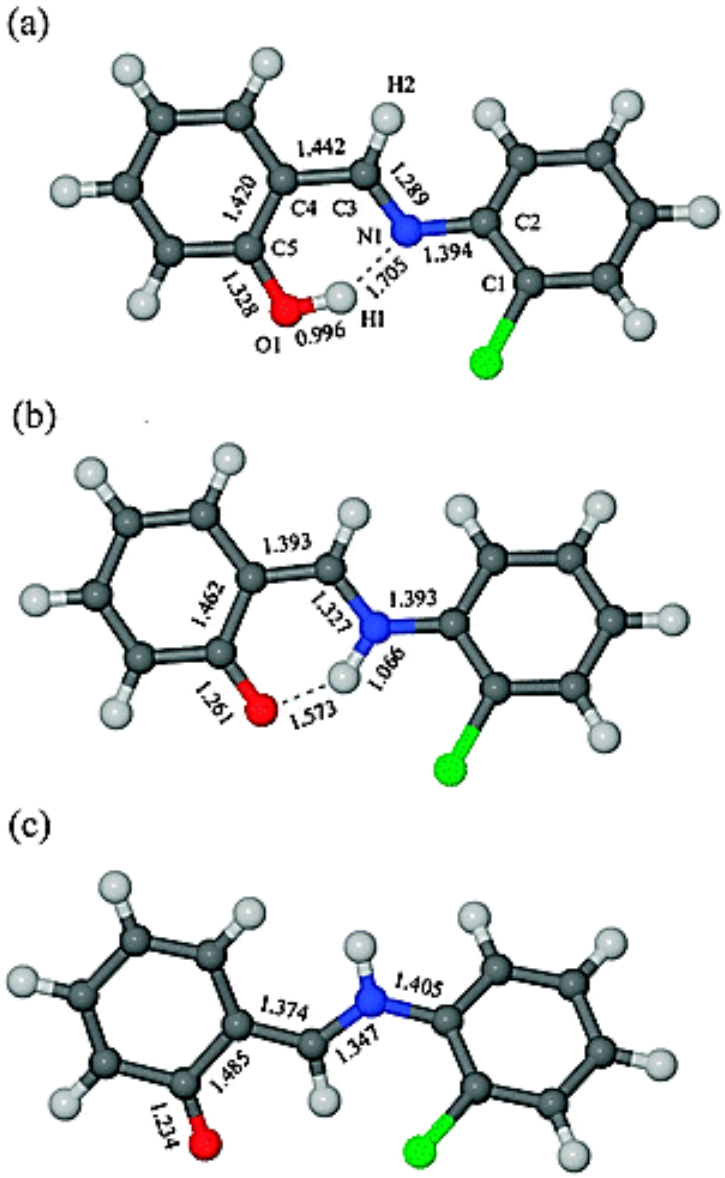

Figure 7. Equilibrium geometries of the isolated ground-state SCA molecule. All distances given in units of Å. (a) *cis*-enol form; (b) *cis*-keto form; (c) *trans*-keto form.

4.2 Photochemical reaction in SCA crystal

The mechanistic course of the photochemical reactions in the SCA crystal was followed with the use of several structural parameters whose definitions we will now present. The proton transfer reaction was monitored through the O1–H1 and N1–H1 distances, and proton transfer was considered to have occurred at the point when these distances became equal. Although in principle it is possible for the shuttling proton to undergo back transfer from nitrogen N1 to oxygen O1, and hence cross through R(O1–H1)=R(N1–H1) more than once, this did not happen in any of the simulated trajectories. Additionally, throughout each simulated

trajectory we kept track of the proton donor–acceptor distance, R(O1–N1). The skeletal deformations of the reactive SCA molecule were monitored by following the four torsion angles which have already been defined in Section 4.1.

In order to detect when the system approaches a conical intersection between the ground- and excited-state potential energy surfaces, throughout each trajectory we also followed the ground-state potential energy of the system, which is defined by:

$$E(S_0) = {}^{PW}E_{DFT}(S) + {}^{GTO}E_{DFT}(C) - {}^{PW}E_{DFT}(C)$$

where ${}^{GTO}E_{DFT}(C)$ stands for the ground-state potential energy of the photoexcited molecule, calculated at the PBE0/6-31G(d,p) level of theory. The system was considered to have reached an S_1/S_0 CI when the potential energy gap between the excited and ground states, $\Delta E = E(S_1) - E(S_0) = {}^{GTO}E_{TD\text{-}DFT}(C) - {}^{GTO}E_{DFT}(C)$, decreased to below the arbitrarily chosen threshold of 0.1 eV. Because of the inability of the TD-DFT method to provide a correct description of the conical intersection region, the simulation was discontinued once the system reached an S_1/S_0 CI, which occurred in every simulated trajectory.

We begin by considering the mechanism of the forward reaction. As will be explained in Sections 4.3.1 and 4.3.2, where two representative trajectories are discussed in detail, the MD trajectories generated on the TD-DFT/DFT potential energy surface revealed two distinct reaction pathways of the photoexcited *cis*-enol molecule. In the first pathway, the molecule undergoes the ESIPT reaction and subsequently reaches an S_1/S_0 conical intersection through a pedal motion of the type predicted by Harada *et al*. The conical intersection reached in the first reaction pathway will from now on be denoted by CIP (short for conical intersection-pedal motion). In the second pathway, the reactive molecule reaches another conical intersection, whose geometry is similar in many respects to the conical intersection CI1 involved in the isolated-molecule reaction mechanism.

The results of all sixteen simulated trajectories of the forward reaction are reviewed in Table 2 below. Proton transfer occurred in seven trajectories within an average of 25 fs of the initial photoexcitation. Following proton transfer, in each of these trajectories the photoexcited molecule persisted in the *cis*-keto form for a period of time, before reaching CIP on average 420 fs after the initial photoexcitation. In the remaining nine trajectories, proton transfer did not take place, and instead the photoexcited molecule reached CI1 on average 110 fs after the initial photoexcitation. From the fact that CI1 is reached very rapidly, we may deduce that this conical intersection is accessible with little or no potential energy barrier. On the other hand, judging from the fact that following the ESIPT reaction, the molecule always persisted in the *cis*-keto form for a few hundred femtoseconds before undergoing the pedal motion, there probably exists a low potential barrier separating the photoexcited *cis*-keto form from the conical intersection CIP.

Trajectory	Outcome[a]	t_{PT},[b] fs	t_{CI1},[b] fs	t_{CIP},[b] fs	$\Delta E(t = 0)$,[c] eV
1	PT, CIP	24.5	—	313.5	3.636
2	PT, CIP	64.5	—	398.0	3.380
3	CI1	—	120.0	—	3.699
4	PT, CIP	33.0	—	349.0	3.645
5	PT, CIP	10.0	—	589.5	3.351
6	CI1	—	88.0	—	3.307
7	PT, CIP	19.5	—	327.0	3.431
8	CI1	—	88.5	—	3.448
9	CI1	—	120.0	—	3.634
10	CI1	—	105.5	—	3.778
11	PT, CIP	24.5	—	570.0	3.586
12	CI1	—	119.0	—	3.323
13	CI1	—	76.5	—	3.466
14	PT, CIP	5.0	—	361.5	3.347
15	CI1	—	160.5	—	3.424
16	CI1	—	110.0	—	3.558

a PT, CI1 and CIP stand for "proton transfer", "reached CI1" and "reached CIP", respectively.*b* t_{PT}, t_{CI1} and t_{CIP} are respectively the time at which proton transfer took place and the time at which the photoexcited molecule reached CI1 and CIP, where $t = 0$ corresponds to the photoexcitation time.*c* $\Delta E(t = 0)$ is the energy gap between the ground state and the first singlet excited state at $t = 0$.

Table 2. Results of simulated trajectories of the forward reaction

Of the eight simulated trajectories of the reverse reaction, which we number 1′ to 8′, two did not reach a conical intersection within a time limit of 1.5 ps, and these simulations were therefore discontinued due to computational time concerns. In each of the remaining six trajectories, the reactive molecule which was initially in the *trans*-keto form reached an S_1/S_0 conical intersection by undergoing a pedal motion. Interestingly, this pedal motion was not simply a reversal of the pedal motion involved in the forward reaction, but rather proceeded in the same direction as the one involved in the forward reaction. (To use the analogy with the pedals of a bicycle, if the forward reaction is a half-turn of the pedals, then the reverse reaction is another half-turn in the same direction, and not a half-turn in the opposite direction.) In order to distinguish it from the conical intersection geometry CIP reached in some of the trajectories of the forward reaction, we will call the S_1/S_0conical intersection reached in the trajectories of the reverse reaction CIP′.

Table 3 summarises the results of the simulated trajectories of the reverse reaction. The lower bound for the average time taken by the system to reach CIP′ was calculated as 980 ps.

Trajectory	**Outcome**[a]	$t_{CIP'}$,[b] **fs**	$\Delta E(t = 0)$,[c] **eV**
1′	CIP′	380.5	2.769
2′	CIP′	1117.5	2.671
3′	CIP′	591.0	2.562
4′	CIP′	665.5	2.958
5′	—	—	2.653
6′	CIP′	829.0	2.701
7′	—	—	2.916
8′	CIP′	1299.0	2.811

a CIP′ stands for "reached CIP′". A dash (—) means that the trajectory did not reach an S_1/S_0 conical intersection within the maximum simulation time of 1.5 ps.
b $t_{CIP'}$ is the time at which the photoexcited molecule reached CIP′, where $t = 0$ corresponds to the photoexcitation time.
c $\Delta E(t = 0)$ is the energy gap between the ground state and the first singlet excited state at $t = 0$.

Table 3. Results of simulated trajectories of the reverse reaction.

In what follows we describe in detail two representative trajectories of the forward reaction, of which one reached CIP and the other CI1, and a single trajectory of the reverse reaction, which reached CIP′. To accompany this narrative, in the ESI‡ we provide a series of animations showing important events in each of these trajectories.

4.2.1 Trajectory 1 of the forward reaction

In trajectory 1, following ESIPT $t = 24.5$ fs, the reactive molecule underwent a pedal motion conformational change and reached CIP at $t = 313.5$ fs, at which point the simulation was terminated.

In Figure 8(a), the ESIPT reaction is analysed by projecting the initial 100 fs of trajectory 1 onto a three-dimensional plot of energy, the proton transfer coordinate defined by R(O1–H1)–R(N1–H1), and the proton donor–acceptor distance coordinate given by R(O1–N1). The energies of both the S_0 and S_1 states are plotted, showing how the energy gap between these two states decreases from 3.636 eV at $t = 0$ to 1.759 eV at $t = 100$ fs.

The projection can be partitioned into segments which correspond to specific events that occur during the initial 100 fs of trajectory 1; these are marked as *a* to*d*. Point *a* is the point at which the initial photoexcitation occurred, and it corresponds to the reactive molecule existing in the *cis*-enol form. Segment *b* is roughly parallel to the proton donor–acceptor distance coordinate, *R*(O1–N1), and corresponds to a shortening of the distance between the two oxygen and nitrogen atoms before the proton transfer step. The next segment *c*, largely parallel to the proton transfer coordinate, is the proton transfer step which converts the photoexcited molecule from the *cis*-enol to the *cis*-keto form. Further along the trajectory, segment *d* marks the beginning of the period when the molecule persists in the *cis*-keto form, which lasts until around $t = 250$ fs. The proton transfer event is also visible as a crossing of the curves *R*(O1–H1) and *R*(N1–H1) in Figure 8(b), which describes the variation in the distances O1–H1, N1–H1 and O1–N1 over the entire trajectory 1.

Figure 8(c), in turn, shows the time-evolution of the four torsion angles which describe the molecular conformation. In this plot the period of time from $t = 0$ to around 250 fs is largely uneventful, exhibiting some small-amplitude oscillations of the four torsion angles but no marked structural change. At around $t = 250$ fs, however, the torsion angles ϕ(N1–C3–C4–C5), ϕ(H2–C3–C4–C5) and ϕ(C1–C2–N1–C3) simultaneously began to change more rapidly in a manner suggesting a concerted twist around the C2–N1 and C3–C4 bonds. This continued until the molecule reached an S_1/S_0 conical intersection at $t = 313.5$ fs.

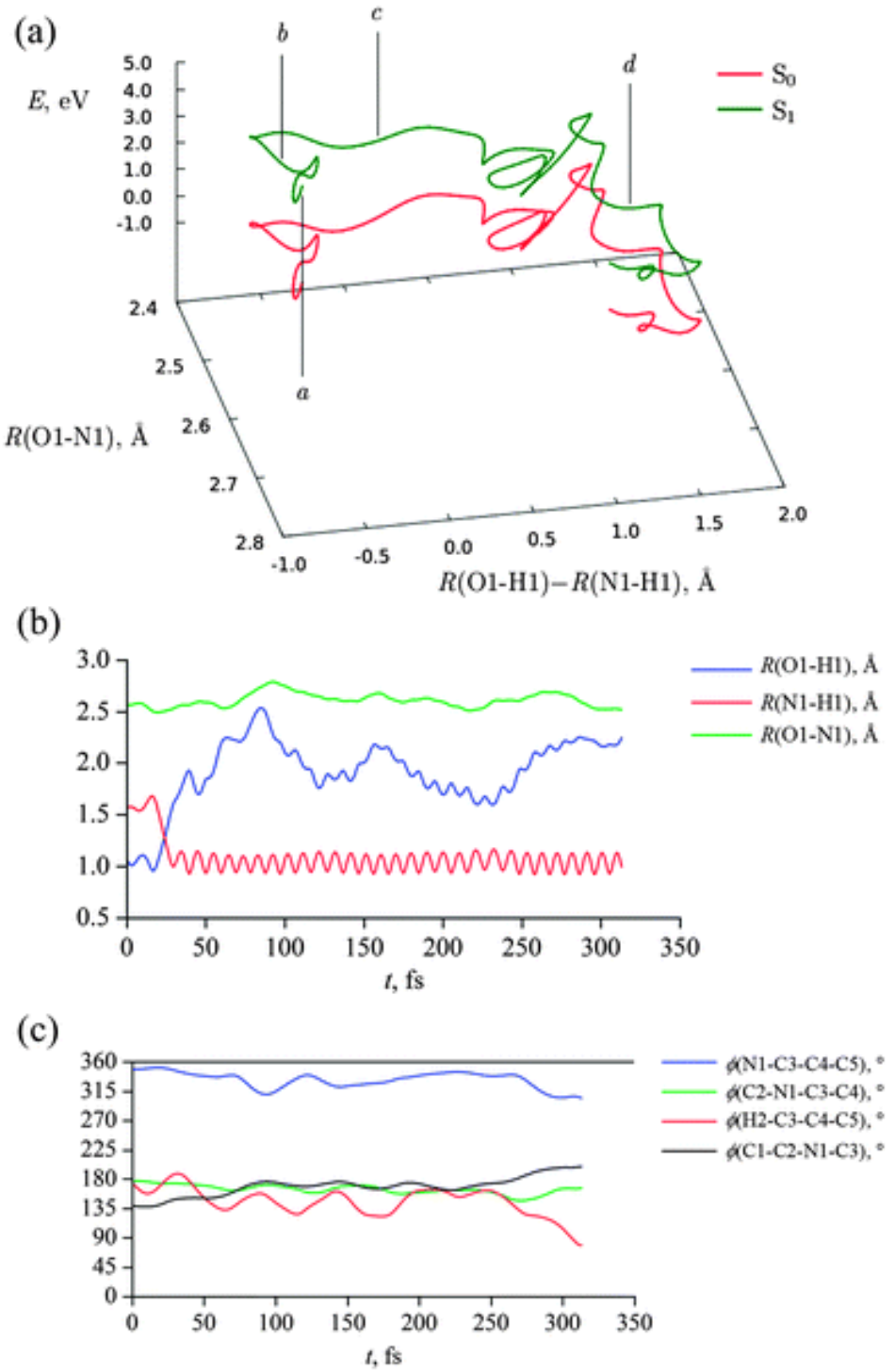

Figure 8. Trajectory 1. (a) Projection of the initial 100 fs of trajectory 1 onto energy, the proton transfer and proton donor–acceptor distance coordinates. The labels *a* to *d* are explained in the text. The zero of the energy scale corresponds to the ground-state energy at the starting point of the trajectory. (b) Time-evolution of the O1–H1, N1–H1 and O1–N1 distances. (c) Time-evolution of the four torsion angles which describe the molecular conformation.

We now turn our attention to the geometry of the system as it reached that conical intersection, which is overlaid on the experimental crystal structure of SCA inFigure 9. The positions of carbon C3 and nitrogen N1 indicate that the photoexcited molecule is in the process of what can confidently be described as a pedal motion, with C3 being located above its crystallographic position while N1 is beneath its crystallographic position (here, 'above' and 'below' refer, of course, to the orientation of the system as illustrated in Figure 9).

From Figure 9 we observe that the surrounding ground-state molecules are all fairly close to their crystallographic positions, which suggests that it is not necessary for the surrounding molecules to become displaced away from the photoexcited molecule in order to make room for the pedal motion.

Through a survey of the other simulated trajectories, it was found that in all trajectories in which the photoexcited molecule underwent proton transfer, it subsequently reached an S_1/S_0 conical intersection through a twisting motion similar to the one that took place in trajectory 1. In each case, carbon C3 moved upwards while nitrogen N1 simultaneously moved downwards, and the values of the torsion angles ϕ(N1–C3–C4–C5) and ϕ(H2–C3–C4–C5) decreased, while concurrently the value of ϕ(C1–C2–N1–C3) increased. We therefore conclude that MD simulations on the TD-DFT/DFT potential energy surface consistently predict that following proton transfer, the photoexcited molecule undergoes a pedal motion, thereby reaching an the S_1/S_0 conical intersection that we denote CIP. Furthermore, the pedal motion is predicted to always proceed in the same direction.

It must be pointed out that this result does not, in itself, prove that by passing through CIP, the reactive molecule undergoes isomerisation to the *trans*-keto form, because after passing through CIP the molecule may also relax back to the *cis*-keto geometry. It seems, however, very unlikely that the *cis*-enol to *trans*-keto photoisomerisation should proceed through a different pathway, because any such pathway would necessarily compete with the very rapid pathway which involves the radiationless de-excitation of the reactive molecule by reaching CIP. Hence, it may be inferred that this reaction proceeds through the mechanism previously proposed through a pedal motion of the type by Harada *et al*.

It is noteworthy that in a recent study by Robert *et al*[10] of the *cis*-enol to *trans*-keto solid-state photoisomerisation reaction of *N*-salicylideneaminopyridines, which are structurally very similar to anils, the pedal motion was not found to be accompanied by the reactive molecule crossing an S_1/S_0 conical intersection. Instead, the pedal motion was predicted to proceed completely in the S_1 state, thus painting a qualitatively different picture of the reaction mechanism. This non-detection of a conical intersection in the work just cited may possibly be attributed to fact that the energies of the S_1 state were calculated using the CI-Singles method, which has the serious drawback of not including electron correlation effects, and it could therefore conceivably give rise a qualitatively incorrect topology of the S_1 potential energy surface.

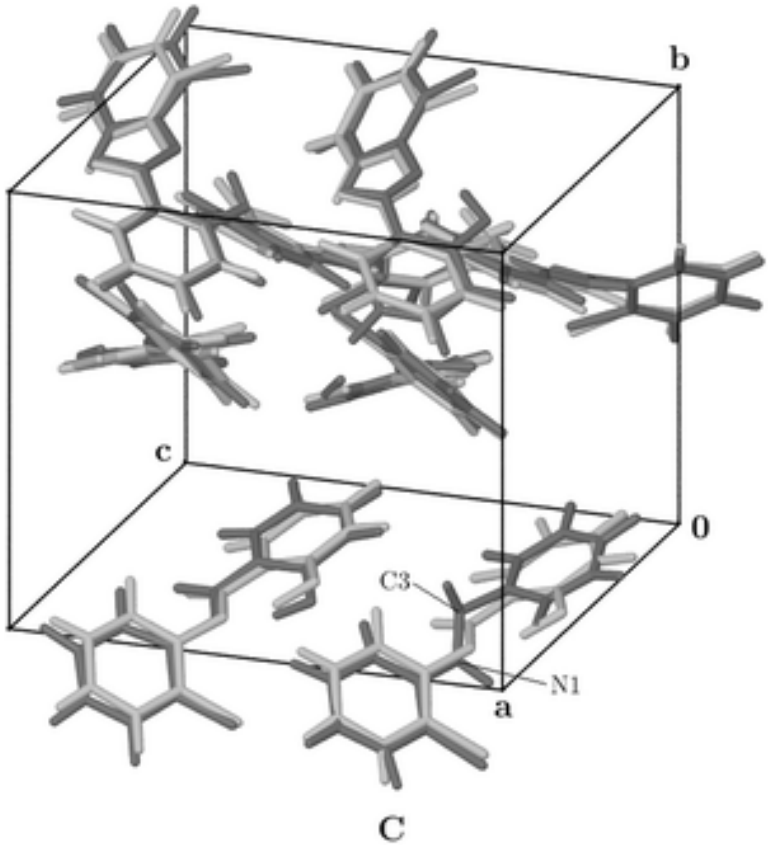

Figure 9. An overlay of the instantaneous configuration of the system on reaching the S_1/S_0 CI in trajectory 1 and the experimental crystal structure of SCA, drawn in dark grey and light grey, respectively. The photoexcited molecule is labelled C.

Lastly, we plot the energies of the S_0 and S_1 states of the reactive molecule, calculated along trajectory 1 at the DFT, TD-DFT and CC2 levels of theory, as a function of time in Figure 10. Visual inspection of this plot reveals that the DFT and CC2 methods provide very similar descriptions of the energy for the S_0 state, whereas for the S_1 state, the TD-DFT and CC2 energies differ on average to a slightly greater extent. This is reflected by the values of the mean absolute deviation between the TD-DFT and CC2 energies, which are 0.16 eV and 0.28 eV for the S_0 and S_1 states, respectively. Overall, however, agreement between the TD-DFT and CC2 excited-state energies is reasonably good. Crucially, in the final part of trajectory 1, both the TD-DFT and CC2 methods predict that the energy gap between the S_0 and S_1 states is progressively decreasing. In particular, at t = 310 fs the energy gap calculated at the at the TD-DFT and CC2 levels was 0.264 eV and 0.396 eV, respectively. Hence, the CC2 method predicts the existence of the conical intersection CIP at the same geometry as the TD-DFT method, lending some additional support to the accuracy of the TD-DFT treatment of the reactive SCA molecule.

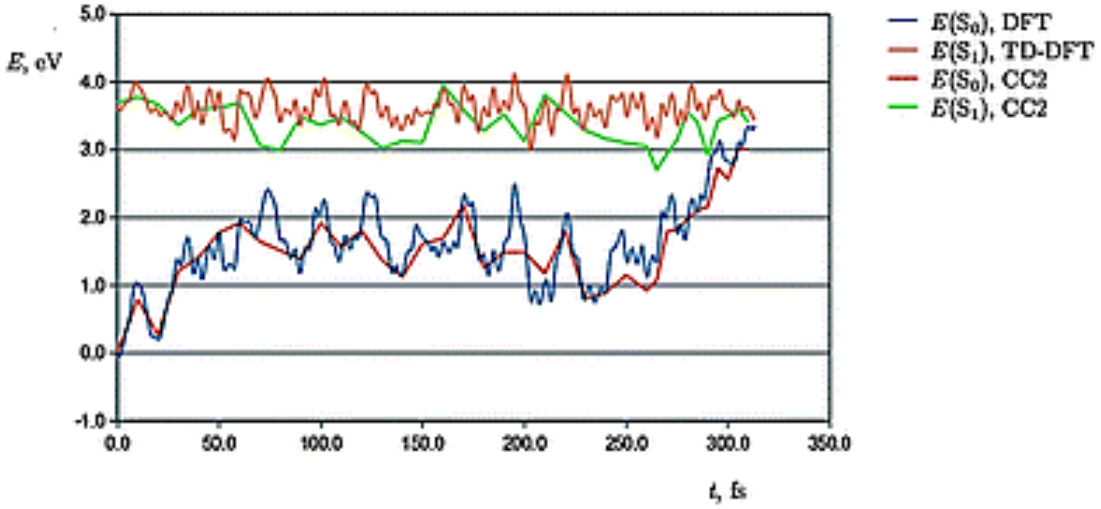

Figure 10. Energies of the S_0 and S_1 states of the photoexcited molecule along trajectory 1, calculated using the DFT, TD-DFT and CC2 methods. The origin of the energy axis is taken at the energy of the S_0 state at t = 0.

4.2.2 Trajectory 3 of the forward reaction

In trajectory 3, the photoexcited molecule reached CI1 at t = 120.0 fs, providing an example of the second reaction pathway of the photochromic polymorph of SCA that leads to the recovery of the starting *cis*-enol form. As evidenced by Figure 11(a), where the distances O1–H1, N1–H1 and O1–N1 are plotted as a function of time, proton transfer did not occur during this trajectory. At around t = 40 fs the N1–H1 and O1–N1 distances began to elongate, until at around t = 100 fs the hydrogen bond of the reactive molecule was nearly ruptured. From around t = 100 fs until the end of the trajectory at t = 120.0 fs, both of these distances were shortening again, indicating the reformation of the hydrogen bond.

In Figure 11(b), we present the time-evolution of the four torsion angles which describe the molecular conformation in the course of trajectory 3. In the period of time from t = 0 to around t = 50 fs, the photoexcited molecule underwent no significant structural changes, but from around t = 50 fs, concurrently with the weakening of the O1–H1···N1 hydrogen bond, the value of torsion angle ϕ(C2–N1–C3–C4) began to undergo a marked decrease, revealing that the molecule was undergoing a torsional motion around the N1–C3 bond. The twisting around this bond (compare Figure 9(c), where the torsion angle ϕ(C2–N1–C3–C4) remains near 180° throughout the entire trajectory 1) and the nonoccurrence of ESIPT indicate clearly that in trajectory 3, the photochemical reaction proceeded in a qualitatively different manner to that in trajectory 1.

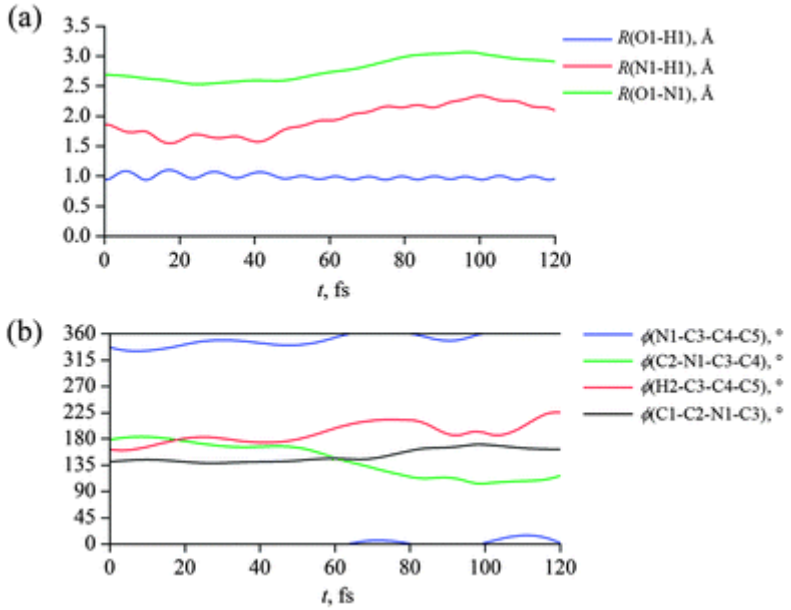

Figure 11. Trajectory 3. (a) Time-evolution of the O1–H1, N1–H1 and O1–N1 distances. (b) Time-evolution of the four torsion angles which describe the molecular conformation.

The outcome of trajectory 3 may be explained by referring to Figure 12, where the final frame from the trajectory, immediately before the S_1/S_0 conical intersection is reached, is overlaid on the experimental crystal structure of the photochromic polymorph of SCA. The reactive molecule exists in a somewhat deformed *cis*-enol conformation, in which the torsion around the N1–C3 bond has moved both the atoms N1 and C3 to below their crystallographic positions. The occurrence of torsion around the N1–C3 bond leading to an S_1/S_0 conical intersection is reminiscent of the photoreaction pathway IC1 predicted previously[16] for the isolated *N*-salicylideneaniline molecule, which leads to the recovery of the initial *cis*-enol form. The fact that in the solid-state reaction of SCA, the salicylidene and chlorophenyl rings do not participate in the torsional motion, but instead remain close to their respective crystallographic positions, can be rationalised by noting that (as explained in Section 2) the crystal structure of the photochromic polymorph of SCA does not contain any large voids, and therefore both rings are constrained to remain near their crystallographic positions. On the basis of the above, we identify the motion observed in trajectory 3 with the IC1 pathway of the isolated molecule.

In Figure 13, the energies of the S_0 and S_1 states of the reactive SCA molecule in trajectory 3, computed using the DFT, TD-DFT and CC2 methods, are plotted as a function of time. Throughout the entire trajectory, the CC2 method very closely reproduces the energies of the S_0 and S_1 states as calculated using the DFT and TD-DFT methods, respectively. The mean absolute deviation in energy between the TD-DFT and CC2 methods is 0.13 eV for the S_0 state and 0.10 eV for the S_1. In consistency with the TD-DFT method, the CC2 method predicts that an S_1/S_0 conical intersection is reached at the end point of trajectory 3.

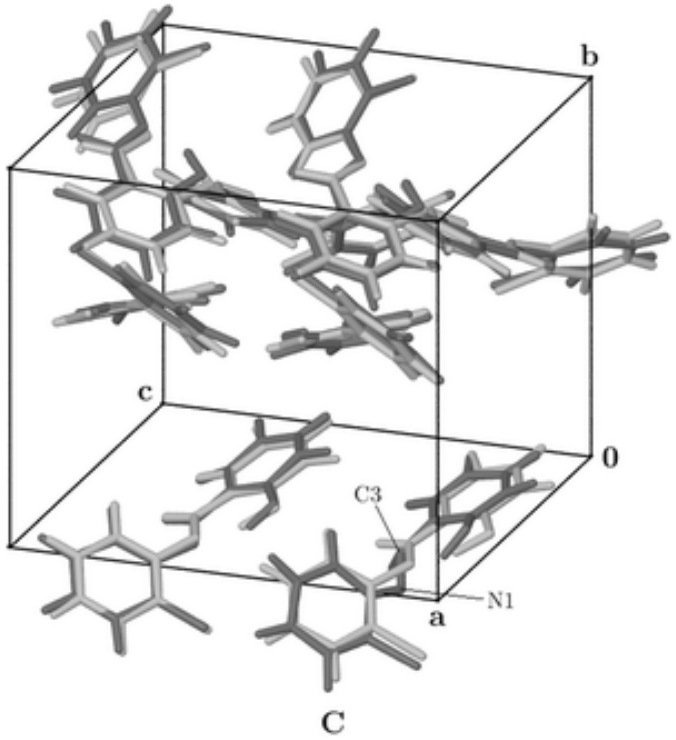

Figure 12. An overlay of the instantaneous configuration of the system on reaching the S_1/S_0 CI in trajectory 3 and the experimental crystal structure of SCA, drawn in dark grey and light grey, respectively. The photoexcited molecule is labelled C.

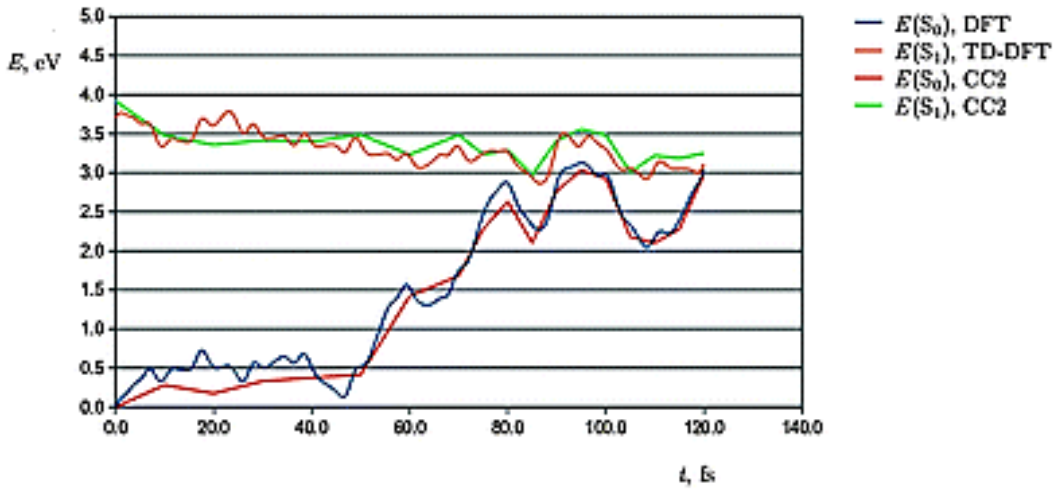

Figure 13. Energies of the S_0 and S_1 states of the photoexcited molecule along trajectory 3, calculated using the DFT, TD-DFT and CC2 methods. The origin of the energy axis is taken at the energy of the S_0 state at t = 0.

4.2.3 Trajectory 3′ of the reverse reaction

In trajectory 3′, following the initial photoexcitation the reactive *trans*-keto molecule persisted with no significant conformational change for around 380 fs before undergoing a pedal motion, which led to it reaching the S_1/S_0 conical intersection geometry which we have termed CIP′.

The time-evolution of the torsion angles ϕ(N1–C3–C4–C5), ϕ(C2–N1–C3–C4), ϕ(H2–C3–C4–C5) and ϕ(C1–C2–N1–C3) along trajectory 3′ is shown inFigure 14. From $t = 0$ to around $t = 380$ fs, all four of these torsion angles remained fairly stable, indicating that the reactive molecule underwent no significant conformational changes during this period. At around $t = 380$ fs, however, the molecule began to undergo a pedal motion, which manifested itself as a gradual decrease of the values of the torsion angles ϕ(N1–C3–C4–C5) and ϕ(H2–C3–C4–C5), and an increase in ϕ(C1–C2–N1–C3), until at $t = 591.0$ fs the reactive molecule reached CIP′. The value of ϕ(C2–N1–C3–C4) was close to 180° throughout the entire trajectory, indicating that the atoms C2, N1, C3 and C4 which connect the two aromatic rings of the reactive molecule remained roughly coplanar while the molecule underwent the pedal motion. A survey of the other trajectories of the reverse reaction shows that these features are typical of all trajectories that reached CIP′, and that in every case, the pedal motion proceeded in the same direction.

It is quite notable that in the forward reaction pathway which involves the reactive molecule reaching CIP through a pedal motion, as shown on the example ofFigure 8(c), the pedal motion also proceeds with a decrease of the values of the torsion angles ϕ(N1–C3–C4–C5) and ϕ(H2–C3–C4–C5), and an increase of the value of ϕ(C1–C2–N1–C3). Thus, we arrive at the surprising conclusion that while the reverse reaction also occurs through a pedal motion, that pedal motion is not a reversal of the one involved in the forward reaction, but proceeds in the same direction. This finding may seem counterintuitive at first, because it might be assumed that the minimum energy pathway for the forward reaction must be the same as the minimum energy pathway for the reverse reaction; if that were the case for the photoisomerisation reaction for SCA, then the pedal motion involved in the reverse reaction would be a reversion of the one that occurs in the forward reaction. However, the above assumption only holds true for reactions that occur in their entirety on single potential energy surfaces. The photoisomerisation of SCA, on the other hand, takes place not on a single potential energy surface, but on two surfaces, such that during the reaction, the molecule undergoes radiationless de-excitation from one surface to another, which renders that assumption invalid. Accordingly, there does not seem to be a theoretical reason to expect that the pedal motions involved in the forward and reverse photoisomerisations must proceed in opposite directions.

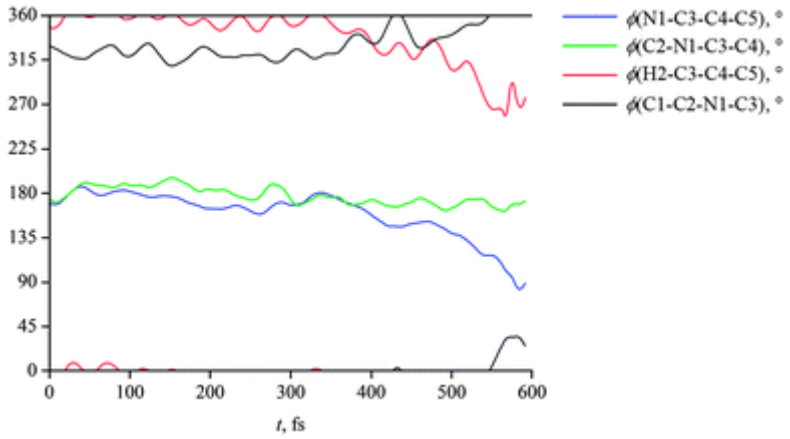

Figure 14. The time-evolution of the four torsion angles which describe the conformation of the reactive molecule in trajectory 3′. (See Figure 7(a) for atom numbering.)

In Figure 15, we present the geometry of the system upon reaching the conical intersection CIP′, overlaid on the experimental crystal structure of SCA. The chlorophenyl ring can be seen to be significantly shifted in its own plane relative to its crystallographic position, while the salicylidene ring is slightly tilted away from its crystallographic position. These displacements likely arose both from the fact that the reactive molecule is in the process of undergoing a pedal motion, as well as from the fact that it started out in the *trans*-keto form, which probably does not "fit" perfectly into the bulk crystal lattice composed of *cis*-enol molecules.

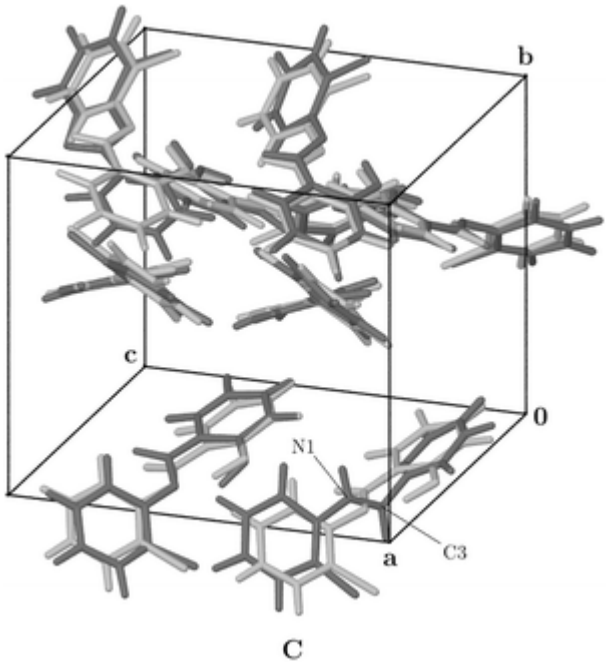

← ***Figure 15.*** An overlay of the instantaneous configuration of the system on reaching the S_1/S_0 CI in trajectory 3′ and the experimental crystal structure of SCA, drawn in dark grey and light grey, respectively. The photoexcited molecule is labelled C.

The atoms N1 and C3 are above and below, respectively, their crystallographic positions, which again shows that the pedal motion through which CIP′ is reached is not a reversal of the pedal motion involved in the forward reaction mechanism, but proceeds in the same direction.

Due to the long duration of trajectory 3′ and the fact that the reactive molecule initially persists in the *trans*-keto form with no significant structural changes, in our assessment of the performance of the TD-DFT method along that trajectory we restrict ourselves to considering its final part. In Figure 16, the energies of the $S_0$and S_1 states of the reactive SCA molecule, computed using the DFT, TD-DFT and CC2 methods, are plotted as a function of time along the final 100 fs of trajectory 3′. It can be seen from Figure 16 that for both states during this period, the agreement between the DFT and TD-DFT energies on the one hand, and the CC2 energies on the other, is only adequate. Indeed, the values of the mean absolute deviation between the DFT, TD-DFT and CC2 energies over this period are fairly high at 0.25 eV and 0.30 eV for the S_0 and S_1 states, respectively. However, in qualitative terms, the TD-DFT and the CC2 method both predict that the reactive molecule is approaching a conical intersection. We therefore believe that the somewhat poor agreement between the energies computed using these two methods is a result of both methods being stretched to the limit when applied to a possibly biradicaloid molecule near a conical intersection, and that it does not represent a qualitative failure of either method.

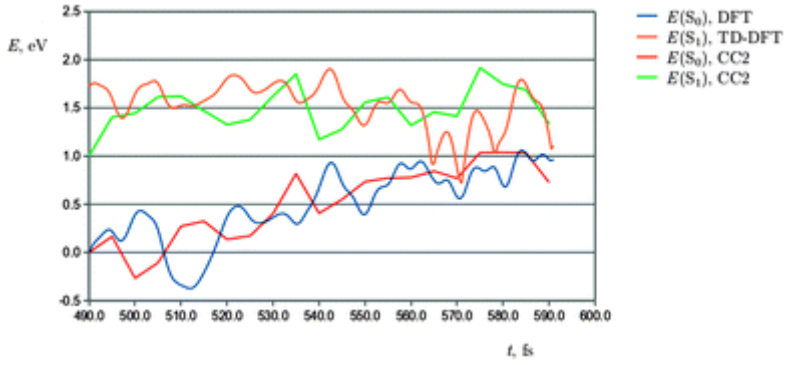

Figure 16. Energies of the S_0 and S_1 states of the photoexcited molecule during the last 100 fs of trajectory 3′, calculated using the DFT, TD-DFT and CC2 methods. The origin of the energy axis is taken at the energy of the S_0 state at t= 490 fs.

5. Conclusions

The photochemical reactions of the photochromic polymorph of the anil *N*-salicylidene-2-chloroaniline were modeled by molecular dynamics simulations employing the hybrid TD-DFT/DFT method to generate the potential energy surface for the solid-state system. It was found that after the initial photoexcitation, the *cis*-

enol isomer has two reaction pathways available to it, which occur with similar probability. The first pathway begins with the ESIPT reaction that converts the photoexcited molecule into the *cis*-keto form. The reactive molecule then persists in the *cis*-keto form, until at an average of 420 fs after the initial photoexcitation event it reaches the conical intersection CIP through a pedal motion (a simultaneous torsion around the C2–N1 and C3–C4 bonds). Because its rapidity precludes the existence of other *cis*-enol to *trans*-keto photoisomerisation pathways, we infer that this pathway is responsible for the photoisomerisation reaction.

The second reaction pathway of the *cis*-enol isomer is analogous to the IC1 reaction channel which has been characterised previously for the isolated *N*-salicylideneaniline molecule, and proceeds through a torsion around the N1–C3 bond, leading to the recovery of the ground state of the starting *cis*-enol form within an average of 110 fs of the initial photoexcitation.

The *trans*-keto isomer, on the other hand, exhibits only a single reaction pathway. Following the initial photoexcitation, the *trans*-keto molecule remains in a largely unchanged conformation for a period of time ranging from a few hundred femtoseconds to over a picosecond, before undergoing a pedal motion in the same direction as the one which occurs in the *cis*-enol to *trans*-keto photoisomerisation. Through this pedal motion, the molecule reaches an S_1/S_0 conical intersection where it undergoes radiationless de-excitation, and proceeds to relax towards either the *cis*-keto or *trans*-keto form on the ground-state potential energy surface.

To the best of our knowledge this is the first report of a molecular dynamics simulation supporting the anil photoisomerisation reaction in the solid state proceeding through a pedal motion.

References

[1] A. Senier and F. G. Shepheard, *J. Chem. Soc.*, 1909, **95**, 1943.

[2] A. Senier, F. G. Shepheard and R. Clarke, *J. Chem. Soc.*, 1912, **101**, 1952.

[3] P. F. Barbara, P. M. Rentzepis and L. E. Brus, *J. Am. Chem. Soc.*, 1980, **102**, 2786.

[4] E. Hadjoudis, J. Argyroglou, E. Lambi and I. Moustakali-Mavridis, *Mol. Eng.*, 1991, **1**, 67–74.

[5] J. Harada, H. Uekusa and Y. Ohashi, *J. Am. Chem. Soc.*, 1999, **121**, 5809.

[6] M. Y. Shen, L. Z. Zhao, T. Goto and A. Mordzinski, *J. Lumin.*, 2000, **87–89**, 667.

[7] N. Otsubo, Ch. Okabe, H. Mori, K. Sakota, K. Amimoto, T. Kawato and H. Sekiya, *J. Photochem. Photobiol., A*, 2002, **154**, 33–39.

[8] E. Hadjoudis and I. M. Mavridis, *Chem. Soc. Rev.*, 2004, **33**, 579.

[9] E. Hadjoudis, A. Rontoyianni, K. Ambroziak, T. Dziembowska and I. M. Mavridis, *J. Photochem. Photobiol., A*, 2004, **162**, 521.

[10] F. Robert, A. D. Naik, B. Tinant, R. Robiette and Y. Garcia, *Chem.–Eur. J.*, 2009, **15**, 4327.

[11] F. Robert, A. D. Naik, F. Hidara, B. Tinant, R. Robiette, J. Wouters and Y. Garcia, *Eur. J. Org. Chem.*, 2010, 621.

[12] K. Johmoto, T. Ishida, A. Sekine, H. Uekusa and Y. Ohashi, *Acta Crystallogr., Sect. B: Struct. Sci.*, 2012, **68**, 297.

[13] F. Robert, P.-L. Jacquemin, B. Tinant and Y. Garcia, *CrystEngComm*, 2012, **14**, 4396.

[14] M. Z. Zgierski and A. Grabowska, *J. Chem. Phys.*, 2000, **112**, 6329.

[15] M. Z. Zgierski and A. Grabowska, *J. Chem. Phys.*, 2000, **113**, 7845.

[16] J. M. Ortiz-Sánchez, R. Gelabert, M. Moreno and J. M. Lluch, *J. Chem. Phys.*, 2008, **129**, 214308.

[17] M. A. Kochman and C. A. Morrison, *J. Chem. Theory Comput.*, 2013, **9**, 1182.

[18] J. Harada, T. Fujiwara and K. Ogawa, *J. Am. Chem. Soc.*, 2007, **129**, 16216.

[19] J. N. Moorthy, P. Mal, R. Natarajan and P. Venugopalan, *J. Org. Chem.*, 2001, **66**, 7013.

[20] L. R. MacGillivray, *J. Org. Chem.*, 2008, **73**, 3311.

[21] F. Toda, *Acc. Chem. Res.*, 1995, **28**, 480.

[22] J. R. Scheffer and W. Xia, *Top. Curr. Chem.*, 2005, **254**, 233.

[23] K. Nakatani and J. A. Delaire, *Chem. Mater.*, 1997, **9**, 2682.

[24] M. Sliwa, S. Létard, I. Malfant, M. Nierlich, P. G. Lacroix, T. Asahi, H. Masuhara, P. Yu and K. Nakatani, *Chem. Mater.*, 2005, **17**, 4727.

[25] S. Park, O.-H. Kwon, S. Kim, S. Park, M.-G. Choi, M. Cha, S. Y. Park and D.-J. Jang, *J. Am. Chem. Soc.*, 2005, **127**, 10070.

[26] J. Bregman, L. Leiserowitz and K. Osaki, *J. Chem. Soc.*, 1964, 2086.

[27] C. F. Macrae, I. J. Bruno, J. A. Chisholm, P. R. Edgington, P. McCabe, E. Pidcock, L. Rodriguez-Monge, R. Taylor, J. van de Streek and P. A. Wood,*J. Appl. Crystallogr.*, 2008, **41**, 466.

[28] H. M. Senn and W. Thiel, *Top. Curr. Chem.*, 2007, **268**, 173.

[29] C. Adamo and V. Barone, *J. Chem. Phys.*, 1999, **110**, 6158.

[30] M. J. Frisch, G. W. Trucks, H. B. Schlegel, G. E. Scuseria, M. A. Robb, J. R. Cheeseman, G. Scalmani, V. Barone, B. Mennucci, G. A. Petersson, H. Nakatsuji, M. Caricato, X. Li, H. P. Hratchian, A. F. Izmaylov, J. Bloino, G. Zheng, J. L. Sonnenberg, M. Hada, M. Ehara, K. Toyota, R. Fukuda, J. Hasegawa, M. Ishida, T. Nakajima, Y. Honda, O. Kitao, H. Nakai, T. Vreven, J. A. Montgomery, Jr., J. E. Peralta, F. Ogliaro, M. Bearpark, J. J. Heyd, E. Brothers, K. N. Kudin, V. N. Staroverov, R. Kobayashi, J. Normand, K. Raghavachari, A. Rendell, J. C. Burant, S. S. Iyengar, J. Tomasi, M. Cossi, N. Rega, J. M. Millam, M. Klene, J. E. Knox, J. B. Cross, V. Bakken, C. Adamo, J. Jaramillo, R. Gomperts, R. E. Stratmann, O. Yazyev, A. J. Austin, R. Cammi, C. Pomelli, J. W. Ochterski, R. L. Martin, K. Morokuma, V. G. Zakrzewski, G. A. Voth, P. Salvador, J. J. Dannenberg, S. Dapprich, A. D. Daniels, Ö. Farkas, J. B. Foresman, J. V. Ortiz, J. Cioslowski and D. J. Fox, *GAUSSIAN 09 (Revision A.02)*, Gaussian, Inc., Wallingford CT, 2009.

[31] J. P. Perdew, K. Burke and M. Ernzerhof, *Phys. Rev. Lett.*, 1996, **77**, 3865.

[32] S. J. Clark, M. D. Segall, C. J. Pickard, P. J. Hasnip, M. J. Probert, K. Refson and M. C. Payne, *Z. Kristallogr.*, 2005, **220**, 567.

[33] Materials Studio CASTEP Online Help. The pseudopotentials used were H_00PBE.usp, C_00PBE.usp, N_00PBE.usp, O_00PBE.usp and Cl_00PBE.usp.

[34] S. Grimme, *J. Comput. Chem.*, 2006, **27**, 1787.

[35] S. Lochbrunner, A. J. Wurzer and E. Riedle, *J. Phys. Chem. A*, 2003, **107**, 10580.

[36] C. Schriever, S. Lochbrunner, A. R. Ofial and E. Riedle, *Chem. Phys. Lett.*, 2011, **503**, 61.

[37] M. Barbatti, A. J. A. Aquino, H. Lischka, C. Schriever, S. Lochbrunner and E. Riedle, *Phys. Chem. Chem. Phys.*, 2009, **11**, 1406.

[38] A. L. Sobolewski and W. Domcke, *J. Chem. Phys. A*, 2007, **111**, 11725.

[39] L. Łapiński, M. J. Nowak, J. Nowacki, M. F. Rode and A. L. Sobolewski, *ChemPhysChem*, 2009, **10**, 2290.

[40] O. Christiansen, H. Koch and P. Jørgensen, *Chem. Phys. Lett.*, 1995, **243**, 409.

[41] TURBOMOLE V6.4 2012, a development of University of Karlsruhe and Forschungszentrum Karlsruhe GmbH, 1989-2007, TURBOMOLE GmbH, since 2007; available from www.turbomole.com.

[42] C. Hättig and F. Weigend, *J. Chem. Phys.*, 2000, **113**, 5154.

[43] C. Hättig, A. Hellweg and A. Köhn, *Phys. Chem. Chem. Phys.*, 2006, **8**, 1159.

[44] T. H. Dunning, *J. Chem. Phys.*, 1989, **90**, 1007.

[45] D. E. Woon and T. H. Dunning, *J. Chem. Phys.*, 1993, **98**, 1358.

[46] R. A. Kendall, T. H. Dunning and R. J. Harrison, *J. Chem. Phys.*, 1992, **96**, 6796.

[47] F. Weigend, A. Köhn and C. Hättig, *J. Chem. Phys.*, 2001, **116**, 3175.